NIH Public Access
Author Manuscript
Small. Author manuscript; available in PMC 2014 May 23.

Published in final edited form as:
Small. 2014 April 24; 10(8): 1623–1633.

Composite RNAi-Microsponges Form through Self-Assembly of the Organic and Inorganic Products of Transcription

Prof. Kevin E. Shopsowitz,
Koch Institute for Integrative Cancer Research, Massachusetts Institute of Technology, Rm 76-553, Cambridge, MA 02139, USA; Department of Chemical Engineering, Massachusetts Institute of Technology, Rm 76-553, Cambridge, MA 02139, USA

Young Hoon Roh,
Koch Institute for Integrative Cancer Research, Massachusetts Institute of Technology, Rm 76-553, Cambridge, MA 02139, USA; Department of Chemical Engineering, Massachusetts Institute of Technology, Rm 76-553, Cambridge, MA 02139, USA

Zhou J. Deng,
Koch Institute for Integrative Cancer Research, Massachusetts Institute of Technology, Rm 76-553, Cambridge, MA 02139, USA; Department of Chemical Engineering, Massachusetts Institute of Technology, Rm 76-553, Cambridge, MA 02139, USA

Stephen W. Morton, and
Koch Institute for Integrative Cancer Research, Massachusetts Institute of Technology, Rm 76-553, Cambridge, MA 02139, USA; Department of Chemical Engineering, Massachusetts Institute of Technology, Rm 76-553, Cambridge, MA 02139, USA

Paula T. Hammond[*]
Koch Institute for Integrative Cancer Research, Massachusetts Institute of Technology, Rm 76-553, Cambridge, MA 02139, USA; Department of Chemical Engineering, Massachusetts Institute of Technology, Rm 76-553, Cambridge, MA 02139, USA

Abstract

Inorganic nanostructures have been used extensively to package nucleic acids into forms useful for therapeutic applications. Here we report that the two products of transcription, RNA and inorganic pyrophosphate, can self-assemble to form composite microsponge structures composed of nanocrystalline magnesium pyrophosphate sheets ($Mg_2P_2O_7{\cdot}3.5H_2O$) with RNA adsorbed to their surfaces. The microsponge particles contain high loadings of RNA (15–21 wt.%) that are protected from degradation and can be obtained through a rolling circle mechanism as large concatemers capable of mediating RNAi. The morphology of the RNAi microsponges is influenced by the time-course of the transcription reaction and interactions between RNA and the inorganic phase. Previous work demonstrated that polycations can be used to condense RNAi microsponges into nanoparticles capable of efficient transfection with low toxicity. Our new

[*]Hammond@mit.edu.

Supporting Information
Supporting Information is available online from the Wiley Online Library or from the author.

NIH-PA Author Manuscript
NIH-PA Author Manuscript
NIH-PA Author Manuscript

NIH-PA Author Manuscript

NIH-PA Author Manuscript

NIH-PA Author Manuscript

findings suggest that the formation of these nanoparticles is mediated by the gradual dissolution of magnesium pyrophosphate that occurs in the presence of polycations. The simple one-pot approach for assembling RNAi microsponges along with their unique properties could make them useful for RNA-based therapeutics.

Keywords

RNAi; self-assembly; nanocomposites; rolling circle transcription; microsponges

1. Introduction

Rolling circle replication (RCR) is a strategy employed by some of the simplest biological entities (e.g., viroids, phages, and plasmids) to efficiently copy their genomes.[1-3] Through the action of a polymerase enzyme continuously traversing a circular template, RCR allows for large linear repeats (concatemers) complementary to the template sequence to be rapidly generated. In addition to its important role in biology, RCR can be carried out in cell-free systems from synthetic circular templates to produce large quantities of DNA or RNA through processes referred to as rolling circle amplification (RCA) and rolling circle transcription (RCT), respectively.[4-6] The rapid and specific isothermal amplification enabled by this technique has led to its use for numerous applications, including the highly sensitive detection of DNA, RNA, and proteins.[7-11].

In addition to its utility for signal amplification and detection, RCR also provides a simple and unique approach for synthesizing large, periodic nucleic acids with interesting properties. By designing appropriate templates, the concatemeric DNA or RNA obtained by RCR can be made to contain high densities of functional units, such as ribozymes, shRNA, and aptamers.[12-15] Recently, researchers have also begun investigating the self-assembly of nucleic acids produced by RCR into diverse nanostructures.[16-21] This has been achieved through different approaches that often employ the rolling circle product as a structural scaffold for other materials, such as complementary nucleic acids, peptides, and inorganic nanoparticles. These exciting applications of RCR could lead to new routes for designing programmable materials with both inherent biological activity and unique structural properties.

Small interfering RNAs (siRNAs) show great potential for the treatment of many diseases due to their ability to inhibit the expression of specific genetic targets.[22-24] The effective use of siRNA as a therapeutic agent, however, requires its efficient packaging in order to facilitate cellular uptake and prevent degradation.[25-28] Several nucleic acid self-assembly approaches, including the use of structural DNA scaffolds and the phi29 pRNA motif, have been employed to generate siRNA-containing nanostructures for *in vivo* delivery.[29-34] Recently, our group reported that RNA synthesized from a circular DNA template resulted in the self-assembly of spherulitic microsponge particles that were shown to contain RNA and were capable of inhibiting gene expression *in vivo* (RNAi microsponges).[35] Herein, we report new findings on the structure, composition, and mechanism of formation for these particles. Our new results demonstrate that these microsponges are composite materials

NIH-PA Author Manuscript

NIH-PA Author Manuscript

NIH-PA Author Manuscript

consisting of RNA and crystalline magnesium pyrophosphate sheets. Self-assembly of the microsponges is driven by the formation of pyrophosphate anions (PPi) during transcription, with structural evolution being related to the kinetics of the RCT reaction combined with interactions between RNA and the inorganic phase. These results shed new light on the formation of RNAi microsponges during RCT and highlight the potential for organic and inorganic molecules generated from a single reaction to coassemble into nanostructures.

2. Results

2.1 Structural Characterization of Microsponges Prepared Using Different DNA Templates

It was previously reported that transcription from a circular DNA template containing a 21 bp double-stranded region in combination with a T7 promoter sequence (referred to as DNA-T1 in the current study) could lead to the formation of particles with microsponge morphology.[35] These particles were found to be nanocrystalline and originally proposed to be composed mostly of RNA. In order to better understand the formation of these microsponge particles, we sought to further investigate the nature of the assembled microstructures, and the influence of the DNA template design on the resulting structures. A dumbbell-shaped DNA molecule with a 21 bp double-stranded region joined by two small single-stranded loops was prepared (DNA-T2), and employed as an alternative template for transcription with T7 RNA polymerase (Scheme 1, otherwise identical versions designed to target GFP or luciferase were used interchangeably throughout the study unless specifically noted). Compared to DNA-T1 (85 bases), DNA-T2 is shorter (57 bases) as it does not contain a promoter sequence (for the specific sequences used in this study, see the Supporting Information). Seyhan et al. previously reported that rolling circle transcription carried out from dumbbell-shaped DNA templates analogous to DNA-T2 yielded large RNA molecules capable of silencing gene expression; however, they did not report the formation of particles from this reaction.[12]

When *in vitro* transcription was carried out from DNA-T2, a white precipitate formed that was isolated by centrifugation after 24 h. This material was examined by scanning electron microscopy (SEM) and transmission electron microscopy (TEM), which revealed ~1-2 μm particles (**Figure 1**) with the microsponge morphology previously observed for particles isolated after transcription from DNA-T1(throughout the rest of the paper, particles generated from DNA-T1 and DNA-T2 will be referred to as MS-1 and MS-2, respectively).[35]

Powder X-ray diffraction (PXRD) was carried out to compare the crystallinity of MS-1 and MS-2 and revealed nearly identical diffraction patterns for the two samples (**Figure 2a**). After further analysis of the diffraction patterns, comparisons to inorganic structural databases ultimately suggested a match with a magnesium pyrophosphate phase, namely $Mg_2P_2O_7 \cdot 3.5H_2O$.[36] The pyrophosphate anion (PPi) is a product of transcription, with one PPi molecule generated for every nucleotide triphosphate that is incorporated into the growing RNA chain. As a result, PPi produced during enzymatic nucleic acid synthesis can react with Mg^{2+} in the reaction buffer to form insoluble magnesium pyrophosphate (Mg_2PP_i).[37] To test this, we prepared a sample of magnesium pyrophosphate by reacting sodium pyrophosphate with an aqueous solution of magnesium chloride using similar

NIH-PA Author Manuscript

NIH-PA Author Manuscript

NIH-PA Author Manuscript

concentrations to those found during RCT; this resulted in the formation of a white precipitate that gave the same X-ray diffraction pattern as MS-1 and MS-2 (Figure 2a). To determine whether the $Mg_2P_2O_7$•$3.5H_2O$ phase is an integral component in the RNAi microsponges, we added pyrophosphatase enzyme to the transcription reaction and found that this prevented the formation of the particles altogether. In addition, we found that the addition of EDTA to the microsponges, which binds strongly to Mg^{2+}, rapidly triggers their dissolution. Taken together with the previous work from our group, these results demonstrate that RNA microsponges produced during RCT are inorganic/RNA composite materials. Although the formation of magnesium pyrophosphate during enzymatic nucleic acid synthesis is known, the co-assembly of this material with RNA into nanostructured particles has not been previously investigated.

2.2 Elemental Analysis of Microsponge Composite Structures

To better understand the structure of the microsponge particles, we used energy dispersive X-ray spectroscopy (EDS) to analyze their elemental composition. Point analysis of the microsponges using EDS reveals the presence of carbon, nitrogen, oxygen, magnesium, and phosphorus, which are all consistent with a mixture of RNA and $Mg_2P_2O_7$(Figure 2b). Elemental quantification was carried out using both wavelength dispersive X-ray spectroscopy (WDS) and X-ray photoelectron spectroscopy (XPS), which yield compositional information related to the bulk (several microns penetration) and surface (several nanometers penetration) of a material, respectively (Figure 2c-d). Using WDS, we found atomic percentages of 4.8% C, 64.5% O, 14.8% Mg, and 15.9% P (nitrogen levels were too low to be accurately quantified). The values for O, Mg, and P are slightly lower than those predicted for $Mg_2P_2O_7$•$3.5H_2O$ (72.4% O, 13.8% Mg, 13.8% P), which is consistent with the added presence of RNA. We note that nearly identical results were obtained for MS-1 and MS-2 samples. When XPS was performed on the same sample, we measured relative atomic percentages of 5.7% N, 24.5% C, 51.1% O, 8.8% Mg, and 9.8% P. The large difference between these values and those obtained by WDS demonstrates that the surface composition of the microsponges is considerably different from their bulk composition. Specifically, the increased presence of carbon and nitrogen, along with the decreased relative amounts of oxygen, magnesium, and phosphorus, suggests that the RNA is enriched at the surface. We proceeded to use scanning transmission electron microscopy (STEM)-based EDS mapping to further study the localization of magnesium pyrophosphate and RNA within the particles. The elemental maps for phosphorus and magnesium (**Figure 3**) show that these elements are concentrated in the sheets that make up the microsponge particles, demonstrating that the sheet nanostructures likely correspond to the crystalline magnesium pyrophosphate phase detected by PXRD. The maps for carbon show a fairly uniform distribution throughout the particles, suggesting an even loading of RNA. Combined with the XPS data, this leads us to propose that RNA is localized at the surfaces of the nanocrystalline $Mg_2P_2O_7$•$3.5H_2O$ sheets that make up the microsponge particles.

2.3 Visualization of RNA within Microsponge Particles and Quantification of RNA Loading

We further examined the localization of RNA within the MS-2 particles by carrying out the transcription reaction in the presence of fluorescent Cy5-labeled UTP, which resulted in a blue precipitate that retained its color even after multiple wash steps. Confocal fluorescence

NIH-PA Author Manuscript

NIH-PA Author Manuscript

NIH-PA Author Manuscript

imaging of this sample shows fluorescent particles with dimensions that match those observed by SEM (**Figure 4a-b**). These images demonstrate that RNA is distributed throughout the particles, in accord with the uniform distribution of carbon observed by EDS mapping. We were also interested in observing what happens to the RNA upon the addition of EDTA, which as mentioned earlier, causes rapid dissolution of the microsponge particles. After the addition of 5 mM EDTA to Cy5-labeled MS-2, the particles began to rapidly change shape, forming spheroid structures, and after ~5 s appeared hollow, suggestive of the formation of RNA capsule structures (Figure 4c). The hollow structures are transient: 10 s following the addition of EDTA the particles had all but disappeared with mainly diffuse fluorescence indicative of free RNA observed (Figure 4d). These results therefore demonstrate that EDTA is capable of rapidly triggering the release of RNA from the microsponge particles.

Thermogravimetric analysis (TGA) was used to determine the loading of RNA within the microsponge particles relative to the inorganic phase. When TGA was performed on the MS-2 particles, we found that ~50 wt. % remained after heating to 600 °C under air (see the Supporting Information, Figure S1). By comparison, 63 wt. % remained after subjecting a control $Mg_2P_2O_7 \cdot 3.5H_2O$ sample (prepared by adding sodium pyrophosphate to the transcription reaction buffer) to the same thermal treatment; from these measurements, we calculate an RNA loading of ~21 wt. %. As an alternative method for determining the weight fraction of RNA in the particles, we measured the total particle mass after drying a given volume of suspension and compared this value to the RNA concentration measured with a fluorescence-based assay (ribogreen). This analysis gave a loading of 15.4±2.5 wt. % RNA, which is comparable to the value obtained by TGA. The RNA quantification measurements were independently carried out on four separate samples (MS-1 and MS-2 synthesized with different [$MgCl_2$] in the buffer), and all yielded values between 12-15 wt. %.

2.4 Time Course of RNA Synthesis and Microsponge Formation

A time-dependent synthesis study was conducted to elucidate the mechanism of particle formation of MS-2 with respect to the time course of the transcription reaction. At each time point of the experiment, particles were isolated and analyzed by SEM and gel electrophoresis (**Figure 5**). In addition, the supernatant was analyzed by electrophoresis and total RNA (supernatant + MS fraction) was quantified using a ribogreen assay to assess the overall reaction progress (Figure 5b). The concentration of RNA produced during the reaction increased continually up until 24 h. The amount of PPi generated during transcription is equivalent to the amount of RNA produced; therefore the concentration of PPi must increase at the same rate as RNA over the course of the reaction. Looking at the supernatant by gel electrophoresis,we see that large transcripts (>1000 bases) are present by two hours (Figure S2). Further, as the RNA concentration increases at later time points (9.5-24 h), the size distribution becomes broader with the upper tail approaching 9000 bases. As a control, when transcription was carried out from the unligated template, we detected a comparatively small quantity of short transcripts (mostly less than 150 bases, see Figure S2b). The observed size distribution of RNA and the dependence on ligation are consistent with concatemeric RNA produced through a rolling circle mechanism.[4, 12, 38]

NIH-PA Author Manuscript

NIH-PA Author Manuscript

NIH-PA Author Manuscript

In comparison to DNA-T2, we found that DNA-T1 yielded substantially shorter transcripts (Figure S3). Although ligation had a significant impact on the yield of RNA produced from DNA-T1, it did not result in transcripts much longer than the size of the template itself. This indicates that ligation is necessary for efficient initiation from this template (the ligation site is in the middle of the T7 promoter sequence). However, processive RCT does not appear to occur from DNA-T1 to the extent that it does from DNA-T2, which could be due to differences in template length and secondary structure, as well as the added presence of the T7 promoter sequence. Given that microsponge particles with the same morphology as those produced from DNA-T2 are obtained from DNA-T1, it appears that the size of the RNA transcripts does not play a major role in defining particle morphology.

To understand the mechanism of particle formation, the solid produced during RCT was isolated at different time points and examined by SEM and DLS (Figure 5b-c and Figure S4). Particles first began to form in the RCT reaction between 2-4 h:at 2 h, we measured a Z avg. diameter of 346 nm by DLS, but were unable to isolate any solid by centrifugation. After 4 h, the Z avg. diameter had shrunk to 205 nm and we were able to isolate small interconnected sheets by centrifugation that had not yet developed into discrete particles (Figure 5c). After 6 h, the Z avg. diameter had again decreased slightly to 123 nm and the solid obtained by centrifugation showed regions of well-defined particles of ~250 nm that resemble miniature versions of the microsponges (Figure 5d). The PPi concentration at this time point was inferred to be ~0.5 mM (based on RNA concentration), which was previously found to be near the minimum detectable concentration for magnesium pyrophosphate-related turbidity during a DNA amplification reaction.[37] By 9.5 h, the particles had grown significantly larger (Z avg. diameter = 3265 nm) and possessed a well-defined microsponge morphology (Figure S4). Finally, as the RNA (and hence PPi) concentration roughly tripled between 9.5-24 h, the size and morphology of the particles did not seem to change substantially. Using gel electrophoresis, we detected RNA in each of the samples isolated during particle formation (Figure 5a); RNA is therefore incorporated into the microsponges throughout the process of their formation. The size distribution of RNA in the microsponges is similar to what is observed in the supernatant; however, at later time points it is less broad and shifted to smaller sizes compared to the supernatant RNA. Overall, we found that ~10-20% of the total RNA produced during RCT was integrated into the microsponges isolated after 24 h.

2.5 Influence of Pyrophosphate Concentration and the Presence of RNA on Magnesium Pyrophosphate Formation

The preceding results temporally resolved the formation of RNAi microsponges as a progression of nucleation of small sheets that grow into larger spheroidal particles as RNA and PPi are generated during RCT. In order to determine the roles of RNA and PPi concentration in governing the microsponge morphology, we added varying concentrations of PPi to $MgCl_2$ solutions in the absence of RNA and isolated the precipitate. When 0.5 mM PPi (roughly equivalent to the 6 h RCT time point) was added to either the transcription reaction buffer or a simple aqueous solution of $MgCl_2$ (16 mM), we observed the formation of ~1 μm spherulitic particles within several hours (Mg_2PPi-0.5, **Figure 6a-b**). These particles consist of slightly larger, more uniform sheets, and generally appear more like

NIH-PA Author Manuscript

NIH-PA Author Manuscript

NIH-PA Author Manuscript

traditional spherulites compared to the sponge morphology that forms during RCT. At lower PPi concentrations, precipitate typically did not form, while at higher concentrations of PPi, we observed different morphologies. When 2 mM PPi was added, aggregates of particles with smaller sheets were obtained that more closely resemble the microsponge precursors seen in Figure 5d; at higher concentrations, the spherulitic morphology was lost altogether (see Figure S5). The addition of RNA (150 μg/mL isolated from the supernatant of a 24 h RCT reaction using DNA-T2) prior to the addition of 0.5 mM PPi, drastically changed the particle morphology compared to the particles formed in the absence of RNA. When RNA was added, after 4 h we isolated a combination of disordered sheets (akin to those isolated at early time points of RCT) and large particles that closely resemble the microsponges obtained during RCT. This result demonstrates that RNA influences the nucleation and growth of magnesium pyrophosphate, suggesting interactions between RNA and the crystalline sheets that may explain how RNA is so readily incorporated into the microsponge particles during RCT.

2.6 RNase Digestion and Transfection of RNA Incorporated in Microsponges

To further assess the localization of RNA within the microsponge particles, we conducted an RNase protection assay. When MS-2 particles were first broken down with EDTA, we found that the released RNA was completely degraded within 6 h by RNase I_f. On the other hand, some short RNA fragments remained after a 24 h RNase I_f treatment of the intact MS-2 particles using the same concentration of enzyme (**Figure 7a**). By observing additional time points, we found that the large RNA molecules contained within MS-2 were fully converted to small fragments within 30 min; however, the small fragments were subsequently degraded more slowly, with 14% remaining after one day. To explain the rapid conversion of RNA within the microsponges to shorter fragments, we conclude that all of the RNA molecules must be accessible; this result is consistent with the hypothesis that the RNA is adsorbed to the surface of the magnesium pyrophosphate sheets that make up the porous microsponge structure. Localization on the surface of the sheets is also consistent with our observation that the morphology of the microsponge particles remained unchanged even after a 48 h RNase treatment (Figure S6). The predicted structure of the RNA generated from DNA-T2 (21 bp double-stranded regions connected by single stranded segments) appears to lead to the rapid generation of dsRNA by RNase I_f, which is selective towards single-stranded RNA. The double-stranded fragments are then broken down more slowly on the surface of the microsponge as compared to when free in solution.

Since the double-stranded region of the RNA generated by RCT is the active component for RNAi, we next tested whether the RNA that remained in the microsponges after treatment with RNase I_f was still active for gene silencing (Figure 7c). MS-2 particles containing a dsRNA sequence targeting GFP were treated with RNase I_f either before or after their dissolution with EDTA. As a positive control, we used the same microsponges without RNase treatment, and, as a negative control, we used microsponges containing a scrambled dsRNA sequence without RNase treatment. The RNase-treated samples were incubated for 1 h at 37 °C prior to heat-inactivation of the RNase enzyme. All of the samples were dissolved with EDTA prior to lipofectamine transfection into a GFP over-expressing SKOV3 cell line. Four days following transfection, the RNase-digested microsponge sample had caused a

NIH-PA Author Manuscript

NIH-PA Author Manuscript

NIH-PA Author Manuscript

40% decrease in GFP fluorescence relative to the scrambled control, while knockdowns of 30% and 4% were observed for the untreated MS-2 sample and the MS-2 sample that was dissolved with EDTA prior to RNase treatment, respectively. These results further suggest that the small fragments produced after the RNase I_f treatment correspond to the active 21 bp double-stranded portion of the RCT transcripts, and that the microsponges protect this active region of the RNA from degradation. The improved silencing caused by the RNase-treated microsponge sample, relative to the positive control, could be attributed to the lipofectamine being optimized for the transfection of siRNA. Additionally, the partially digested RNA molecules may not require further intracellular processing by Dicer, which is believed to be necessary for concatemeric siRNA.[12]

2.7 Interaction of RNA Microsponges and Magnesium Pyrophosphate with Polyethylene Imine

In our previous work, we found that the addition of linear polyethylene imine (LPEI) to RNA microsponges resulted in the formation of ~200 nm condensed particles. In order to test what happens to the inorganic Mg_2PPi phase in the presence of LPEI, we added varying concentrations of LPEI to aqueous suspensions of the Mg_2PPi particles formed without RNA. From DLS, we observed a gradual decrease in the size of the particles that depended on the amount of LPEI added. For example, when a 5 mg/mL PEI solution was used (the same concentration previously employed to condense the RNA microsponges),[35] the size of the Mg_2PPi particles decreased from > 1μm to ~200 nm over the course of 18 h. The remaining solid was isolated by centrifugation and analyzed by SEM and EDS, which reveals the destruction of the original spherulitic particles into disordered magnesium pyrophosphate aggregates (Figure S7). These results demonstrate that the conditions previously used to condense RNA microsponges are also capable of breaking down pure magnesium pyrophosphate particles.

3. Discussion

Our new findings indicate that RNAi microsponges are self-assembled composite structures that form through the simultaneous generation of nanocrystalline sheets of $Mg_2P_2O_7{\bullet}3.5H_2O$ and RNA during transcription. A variety of characterization techniques suggest that large quantities of RNA are adsorbed onto the surface of the nanocrystalline sheets: based on TGA and fluorescence-based RNA assays, the weight fraction of RNA in the microsponges ranges from ~15 to 21%, which compares favorably to other inorganic particle systems that have been used for siRNA delivery.[39] The growth of the microsponge particles proceeds through the initial formation of disordered nanosheet networks at low concentrations of PPi and RNA that gradually form larger spheroidal microsponges as RNA and PPi are produced during transcription. We found that RNA appears to be incorporated into the structures early on in the growth process and influences the resulting morphology. Taken together, these observations lead us to speculate that RNA provides nucleation sights for the growth of the magnesium pyrophosphate phase. While it remains unknown what the precise interactions are between the RNA and the $Mg_2P_2O_7{\bullet}3.5H_2O$ crystal faces, it seems plausible that they are facilitated by the chemical similarity between pyrophosphate and the RNA sugar-phosphate backbone.

NIH-PA Author Manuscript

NIH-PA Author Manuscript

NIH-PA Author Manuscript

RNase digestion experiments reveal that the concatemeric RNA present within the microsponges is highly accessible as evidenced by its rapid conversion to short fragments; this accessibility is likely related to the highly porous structure of the particles. On the other hand, localization within the RNA microsponges protects the fragments against further degradation compared to free RNA. The small fragments produced after RNase I_f treatment of the microsponges are still highly active for gene knockdown, which suggests that they correspond to the double-stranded siRNA region encoded by the DNA template that was employed. The protection of these regions may be in part due to the nature of the interactions between the RNA and the $Mg_2P_2O_7{\bullet}3.5H_2O$ nanocrystals; additional studies are expected to further elucidate the nature of the RNA arrangement on the surface and how this relates to its protection from degradation.

In our previous work we found that when polycations, such as LPEI, were added to the RNAi microsponges they would ‘condense’ into smaller nanoparticles approximately 200 nm in size. The resulting nanoparticles exhibited high transfection rates at low concentrations of nanoparticle and it was postulated that the resulting nanoparticles contained a large number of siRNA copies compared to typical polyplexes. With our added understanding of the microsponge structure, one possibility is that when the microsponges are exposed to polycation solutions, the magnesium pyrophosphate scaffold is deconstructed through competitive complexation of ions, and the negatively charged micron-scale particle is condensed into a nanoparticle that contains the RNA previously sequestered on the nanostructured microsponge surfaces. We have observed that the addition of LPEI leads to a gradual dissolution of the magnesium pyrophosphate particles formed directly by combining sodium pyrophosphate and magnesium chloride. We hypothesize that nanoparticles produced through the simultaneous RNA condensation and crystallite deconstruction of the inorganic component of the microsponges may form via a different pathway than traditional polyplexes, yielding potent nanoscale transfection agents with low polycation-based toxicity. In addition, the size and structure of the RNA produced through RCT might also influence the properties of the resulting nanoparticles; future work will aim to better understand how these different factors contribute towards the formation and biological activity of these materials.

Findings from this work suggest that the yield and structure of microsponge particles formed during RCT can be controlled through the manipulation of assembly conditions. Currently, the amount of RNA produced during the rapid RCT process greatly exceeds the loading capacity of the microsponges that are simultaneously produced; in the supernatant, we find high concentrations of RNA. The results presented herein, however, suggest that the yield of microsponge particles can be improved by simply adding an additional source of PPi at the appropriate concentration. We are currently investigating this avenue to increase the number of available sponges for co-assembly and loading of RNA, which may provide a route to much greater amounts of self-assembled RNAi microsponge structures for delivery. Future work will also entail manipulating the size of microsponges by changing the reaction conditions to control the number of initiating events that cause sponge nucleation.

NIH-PA Author Manuscript

NIH-PA Author Manuscript

NIH-PA Author Manuscript

4. Conclusions

We have presented a detailed investigation regarding the mechanism of formation and composition of self-assembled microsponges that form during RCT. Our results reveal that the microsponges are composite materials produced through interactions between RNA and magnesium pyrophosphate generated during transcription. These materials together form complex sheet networks that further assemble into nanostructured microparticles. We found that the RNAi microsponges consist of between 15 to 21% RNA by weight, with the remainder consisting of a nanocrystalline magnesium pyrophosphate phase identified as $Mg_2P_2O_7{\cdot}3.5H_2O$. These inorganic sheets provide a high surface area for the presentation of concatemeric RNA molecules capable of silencing gene expression. The RNA molecules localized in the microsponge structures are protected from degradation, can be rapidly released in response to a specific stimulus (EDTA), and are accessible for further complexation with polycations. It is proposed that the microsponges may act to concentrate RNA in a form that can ultimately be complexed with polycations to obtain nanoparticles with high relative siRNA content for delivery applications. Furthermore, this system sheds light on how interactions between inorganic and organic products of a single reaction can lead to the assembly of composite nanostructures.

5. Experimental

General

All reagents were purchased from commercial sources and used as received. The plasticware and water used for all of the experiments were certified RNase and DNase free. T4 DNA ligase, T7 RNA polymerase, NTP solutions, RNase I_f, and the corresponding buffers were purchased from New England Biolabs (NEB). PAGE-purified, 5′-phosphorylated DNA templates were purchased from Integrated DNA Technologies. Dynamic light scattering and zeta-potential measurements were carried out using a Malvern Nano-ZS90 zetasizer. Samples for powder X-ray diffraction (PXRD) were prepared by dropcasting onto small pieces of copper tape. PXRD measurements were collected using a Rigaku SmartLab equipped with a 9 kW rotating anode copper source. Data was collected from 5 to 40° 2θ in a parallel beam configuration with ω fixed at 1° to facilitate measurements from limited sample quantities. Gel electrophoresis was run on 1.5-2% agarose gels containing GelRed™ in TBE buffer. Samples were prepared using a formamide-containing RNA loading dye (NEB) according to the manufacturer's protocol. Gels were run at 3 V/cm and visualized using a UV transilluminator. SKOV3 human ovarian carcinoma cells were obtained from ATCC and were cultured according to the provided guidelines. A lentivirus containing a GFP vector was purchased from Cell Biolabs Inc., and was used to make stable GFP-expressing SKOV3 cells according to the vendor's instruction. Lipofectamine was purchased from Invitrogen.

Ligation of DNA Templates

Ligation of DNA-T1 was carried out using a slight modification of a previously published procedure. Briefly, the 5′-phosphorylated ssDNA template (0.5 μM) and an ssDNA splint (1.5 μM) corresponding to the T7 promoter region were combined at a 1:3 molar ratio in the

NIH-PA Author Manuscript

NIH-PA Author Manuscript

NIH-PA Author Manuscript

ligation reaction buffer (66 mM Tris-HCl, 10 mM $MgCl_2$, 1 mM DTT, 1 mM ATP, 7.5% PEG 6000, pH 7.6). The two DNA fragments were annealed by heating to 95 °C for 2 min prior to allowing the solution to cool to 20 °C over the course of ~2 h. Ligation was carried out by adding T4 DNA ligase (1000 U/100 μL reaction) followed by incubation at 20 °C for 2 h. For DNA-T2, a similar procedure was used except that the splint DNA was omitted and a higher concentration of the ssDNA (2.2 μM) was used.

Synthesis of RNAi Microsponges

For a typical reaction, 120 μL of the unpurified reaction mixture containing ligated DNA-T1 or DNA-T2, 29 μL of water, 20 μL of 10× T7 RNA polymerase reaction buffer (NEB), 5 μL of 80 mM NTP solution, and 6 μL of 200 mM $MgCl_2$ were combined and mixed thoroughly prior to the addition of 20 μL of T7 RNA polymerase (50 U/μL). The reaction was incubated at 37 °C for 24 h (or shorter for time-course experiments) at which point the reaction mixture was briefly sonicated and the white solid that had formed was isolated by centrifugation at 1200 × g for 10 min. The resulting pellet was washed three times with 200 μL of water and resuspended in the same volume of water to give MS-1 or MS-2. For the synthesis of Cy5-labelled RNAi MS, the exact same procedure was followed excepted that Cy5-UTP (Enzo Life Sciences) was added to a final concentration of 0.2 mM.

Synthesis of Magnesium Pyrophosphate Control Samples

Magnesium pyrophosphate control samples were synthesized by adding varying amounts of a freshly prepared 50 mM solution of $Na_4P_2O_7 \cdot 10H_2O$ (Sigma) to 1× T7 RNA polymerase buffer solution containing 16 mM $MgCl_2$. Samples were incubated at 37 °C for 4-24 h, isolated by centrifugation for 10 min at 1200 × g, and washed three times with DI-water. Alternatively, a pure aqueous solution of 16 mM $MgCl_2$ (Sigma) was used in place of the buffer solution, which gave particles with the same morphology. PXRD demonstrated that these samples contained the same magnesium pyrophosphate phase as the RNAi microsponge samples, namely $Mg_2P_2O_7 \cdot 3.5H_2O$

Electron Microscopy and Compositional Analysis

Scanning electron microscopy (SEM) images were captured using a JEOL 6700F SEM. Samples were prepared by drop-casting aqueous suspensions onto silicon wafers and were imaged without sputter-coating, typically at an accelerating voltage of 2 kV. TEM images were collected using a JEOL 2010 TEM at an accelerating voltage of 200 kV. EDS maps were collected on a JEOL 2010F TEM equipped with an analytical scanning imaging device (ASID) and INCA EDS detector using a 1 nm probe.Chemical compositions were obtained through wavelength dispersive X-ray spectrometry (WDS) on a JEOL JXA-8200 Superprobe electron probe micro-analyzer (EPMA) at MIT. Data were acquired at an accelerating voltage of 15 kV using a 4 μm probe diameter. Quantification was carried out by averaging data collected from 10 locations and using a graphite standard for carbon, an apatite standard for oxygen and phosphorus, and a diopside-jadeite mineral standard for magnesium. XPS spectra were collected with a Physical Electronics Versaprobe II X-ray Photoelectron Spectrometer. Quantification was carried out by averaging data from three spectra, each collected using a 200 μm spot size.

NIH-PA Author Manuscript

NIH-PA Author Manuscript

NIH-PA Author Manuscript

Thermogravimetric Analysis and RNA Quantification

Thermogravimetric analysis was performed with a TA Instruments Discovery Thermogravimetric Analyzer. All samples were run under flowing air and heated at a rate of 10 °C/min. The wt. % RNA in the microsponge samples was calculated using two different methods. The first method consisted of gravimetrically determining the total mass/volume RNAi MS concentration by drying a given volume of suspension in the TGA at 90 °C until the weight became stable. The RNA concentration was measured for the same RNAi MS sample using a RiboGreen® RNA assay kit (Invitrogen) according to the manufacturer's protocol (this assay was done using an EDTA-containing buffer, which we have found dissolves the particles and releases the RNA). Fluorescence was measured using a Tecan Infinite M200 Pro 96-well plate reader and concentration was calculated based on an RNA standard curve. RNA wt. % was then calculated by dividing the RNA concentration by the gravimetric particle concentration. Measurements were carried out in triplicate for four independent samples. Alternatively, RNA wt. % was determined by comparing TGA curves for RNAi microsponge and magnesium pyrophosphate control samples heated to 600 °C under air. The difference in weight loss for these two samples (more weight loss occurred for the RNAi MS sample) was assumed to correspond to the RNA content of the RNAi microsponges; RNA wt. % was therefore calculated by dividing this difference by the final wt. % of the control sample.

Confocal Microscopy

Cy5-labeled RNAi microsponges were imaged using a Nikon A1R Ultra-Fast Spectral Scanning Confocal Microscope with a 40X objective at room temperature (Nikon instruments Inc., Melville, NY). Microsponges were imaged in situ in a CELLview glass bottom dish (Greiner Bio-One GmbH, Germany). EDTA was added to the microsponge sample at a concentration of 5 mM followed by temporally resolved imaging of its effect on the microsponge particles. Imaging conditions remained constant throughout the experiment.

RNase Digestion and Transfection of RNAi Microsponges

RNase I_f digestions were carried out by adding 100 units of enzyme to a 20 μL volume of 1× reaction buffer (NEBuffer 3) containing RNAi MS particles with ~1 μg RNA. The reactions were incubated at 37 °C and terminated by heat deactivation at 70 °C for 10 min. For the EDTA-treated samples, 4 μL of 50 mM EDTA were added prior to the addition of the enzyme. For the intact MS-2 samples, EDTA was added after heat deactivation of RNase I_f in order to release the RNA prior to transfection. GFP-expressing SKOV3 cells were transfected with RNAi microsponge samples to investigate target gene silencing after RNase treatment. For a positive control, an RNAi microsponge sample without RNase treatment was used and for a negative control, we employed an RNAi microsponge sample not targeted against GFP (scrambled control). Briefly, EDTA-dissolved RNAi miscrosponge samples were complexed with the lipofectamine® transfection reagent. The complexes were prepared according to the manufacturer's protocol. The cells were first seeded in a 96-well plate at 30% confluence and after 24 h were treated with the lipoplex samples at 3 pmol RNA (based on the 21 bp portion) per well. Four days post transfection, the cells were harvested with trypsin and the cell-associated GFP fluorescence was assessed by flow

NIH-PA Author Manuscript

NIH-PA Author Manuscript

NIH-PA Author Manuscript

cytometry (excitation 480 nm; emission 530 nm) using a BD LSRFortessa flow cytometer coupled with a high-throughput system for the 96-well plate format (BD biosciences, San Jose, CA).

Supplementary Material

Refer to Web version on PubMed Central for supplementary material.

Acknowledgments

We would like to acknowledge funding, in part, by the Koch Institute Support (core) Grant P30-CA14051 from the National Cancer Institute as well as the Center for Cancer Nanotechnology Excellence (CCNE), grant number: 5 U54 CA151884-02. We would also like to thank the Koch Institute for Integrative Cancer Research at MIT for providing facilities to support this work. We thank the Koch Institute Swanson Biotechnology Center for technical support, specifically the microscopy and flow cytometry cores. This work also made use of the MIT MRSEC Shared Experimental Facilities supported by the National Science Foundation under award number DMR-0819762. We would also like to thank Dr. Nilanjan Chatterjee and the MIT Electron Microprobe Facility for assistance with WDS analysis.

K.E.S. would like to acknowledge a National Sciences and Engineering Research Council (NSERC) postdoctoral fellowship. J.Z.D. would like to acknowledge a CJ Martin Fellowship supported by National Health and Medical Research Council, Australia. S.W.M. would like to acknowledge a National Science Foundation Graduate Research Fellowship (NSF GRF).

References

[1]. Rochaix JD, Bird A, Bakken A. J. Mol. Biol. 1974; 87:473. [PubMed: 4444033]

[2]. Rasooly A, Rasooly RS. Trends Microbiol. 1997; 5:440. [PubMed: 9402700]

[3]. Flores R, Grubb D, Elleuch A, Nohales M-A, Delgado S, Gago S. RNA Biol. 2011; 8:200. [PubMed: 21358283]

[4]. Daubendiek SL, Ryan K, Kool ET. J. Am. Chem. Soc. 1995; 117:7818.

[5]. Liu DY, Daubendiek SL, Zillman MA, Ryan K, Kool ET. J. Am. Chem. Soc. 1587; 1996

[6]. Fire A, Xu SQ. Proc. Natl. Acad. Sci. U. S. A. 1995; 92:4641. [PubMed: 7753856]

[7]. Lizardi PM, Huang XH, Zhu ZR, Bray-Ward P, Thomas DC, Ward DC. Nat. Genet. 1998; 19:225. [PubMed: 9662393]

[8]. Baner J, Nilsson M, Mendel-Hartvig M, Landegren U. Nucleic Acids Res. 1998; 26:5073. [PubMed: 9801302]

[9]. Schweitzer B, Wiltshire S, Lambert J, O'Malley S, Kukanskis K, Zhu ZR, Kingsmore SF, Lizardi PM, Ward DC. Proc. Natl. Acad. Sci. U. S. A. 2000; 97:10113. [PubMed: 10954739]

[10]. Schweitzer B, Roberts S, Grimwade B, Shao WP, Wang MJ, Fu Q, Shu QP, Laroche I, Zhou ZM, Tchernev VT, Christiansen J, Velleca M, Kingsmore SF. Nat. Biotechnol. 2002; 20:359. [PubMed: 11923841]

[11]. G, Kumar,; G, Chernaya,. BioTechniques. 2009; 47:637. [PubMed: 19594449]

[12]. Seyhan AA, Vlassov AV, Johnston BH. Oligonucleotides. 2006; 16:353. [PubMed: 17155910]

[13]. Zhao W, Cui CH, Bose S, Guo D, Shen C, Wong WP, Halvorsen K, Farokhzad OC, Teo GSL, Phillips JA, Dorfman DM, Karnik R, Karp JM. Proc. Natl. Acad. Sci. U. S. A. 2012; 109:19626. [PubMed: 23150586]

[14]. Daubendiek SL, Kool ET. Nat. Biotechnol. 1997; 15:273. [PubMed: 9062929]

[15]. Cheglakov Z, Weizmann Y, Braunschweig AB, Wilner OI, Willner I. Angew. Chem. Int. Ed. 2008; 47:126.

[16]. Zhao W, Ali MM, Brook MA, Li Y. Angew. Chem. Int. Ed. 2008; 47:6330.

[17]. Lin C, Wang X, Liu Y, Seeman NC, Yan H. J. Am. Chem. Soc. 2007; 129:14475. [PubMed: 17963390]

NIH-PA Author Manuscript

NIH-PA Author Manuscript

NIH-PA Author Manuscript

[18]. Hamblin GD, Carneiro KMM, Fakhoury JF, Bujold KE, Sleiman HF. J. Am. Chem. Soc. 2012; 134:2888. [PubMed: 22283197]

[19]. Wilner OI, Orbach R, Henning A, Teller C, Yehezkeli O, Mertig M, Harries D, Willner I. Nat. Commun. 2011; 2

[20]. Ma Y, Zheng H, Wang C, Yan Q, Chao J, Fan C, Xiao S-J. J. Am. Chem. Soc. 2013; 135:2959. [PubMed: 23414516]

[21]. Zhao W, Gao Y, Kandadai SA, Brook MA, Li Y. Angew. Chem. Int. Ed. 2006; 45:2409.

[22]. Ryther RCC, Flynt AS, Phillips JA, Patton JG. Gene Ther. 2005; 12:5. [PubMed: 15496962]

[23]. Behlke MA. Mol. Ther. 2006; 13:644. [PubMed: 16481219]

[24]. de Fougerolles A, Vornlocher H-P, Maraganore J, Lieberman J. Nat. Rev. Drug Discovery. 2007; 6:443.

[25]. Akhtar S, Benter IF. J. Clin. Invest. 2007; 117:3623. [PubMed: 18060020]

[26]. Whitehead KA, Langer R, Anderson DG. Nat. Rev. Drug Discovery. 2009; 8:129.

[27]. Gilleron J, Querbes W, Zeigerer A, Borodovsky A, Marsico G, Schubert U, Manygoats K, Seifert S, Andree C, Stoeter M, Epstein-Barash H, Zhang L, Koteliansky V, Fitzgerald K, Fava E, Bickle M, Kalaidzidis Y, Akinc A, Maier M, Zerial M. Nat. Biotechnol. 2013; 31:638. [PubMed: 23792630]

[28]. Sahay G, Querbes W, Alabi C, Eltoukhy A, Sarkar S, Zurenko C, Karagiannis E, Love K, Chen D, Zoncu R, Buganim Y, Schroeder A, Langer R, Anderson DG. Nat. Biotechnol. 2013; 31:653. [PubMed: 23792629]

[29]. Lee H, Lytton-Jean AKR, Chen Y, Love KT, Park AI, Karagiannis ED, Sehgal A, Querbes W, Zurenko CS, Jayaraman M, Peng CG, Charisse K, Borodovsky A, Manoharan M, Donahoe JS, Truelove J, Nahrendorf M, Langer R, Anderson DG. Nat. Nanotech. 2012; 7:389.

[30]. Severcan I, Geary C, Verzemnieks E, Chworos A, Jaeger L. Nano Lett. 2009; 9:1270. [PubMed: 19239258]

[31]. Shu Y, Cinier M, Fox SR, Ben-Johnathan N, Guo P. Mol. Ther. 2011; 19:1304. [PubMed: 21468002]

[32]. Shu Y, Haque F, Shu D, Li W, Zhu Z, Kotb M, Lyubchenko Y, Guo P. RNA. 2013; 19:767. [PubMed: 23604636]

[33]. Guo P, Haque F, Hallahan B, Reif R, Li H. Nucleic Acid Ther. 2012; 22:226. [PubMed: 22913595]

[34]. Lee S, Chung B, Park T, Nam Y, Mok H. Acc. Chem. Res. 2012; 45:1014. [PubMed: 22413937]

[35]. Lee JB, Hong J, Bonner DK, Poon Z, Hammond PT. Nat. Mater. 2012; 11:316. [PubMed: 22367004]

[36]. Kongshaug KO, Fjellvag H, Lillerud KP. Solid State Sci. 2000; 2:205.

[37]. Mori Y, Nagamine K, Tomita N, Notomi T. Biochem. Biophys. Res. Commun. 2001; 289:150. [PubMed: 11708792]

[38]. Seidl CI, Ryan K. Plos One. 2011; 6

[39]. Hom C, Lu J, Liong M, Luo H, Li Z, Zink JI, Tamanoi F. Small. 2010; 6:1185. [PubMed: 20461725]

NIH-PA Author Manuscript
NIH-PA Author Manuscript
NIH-PA Author Manuscript

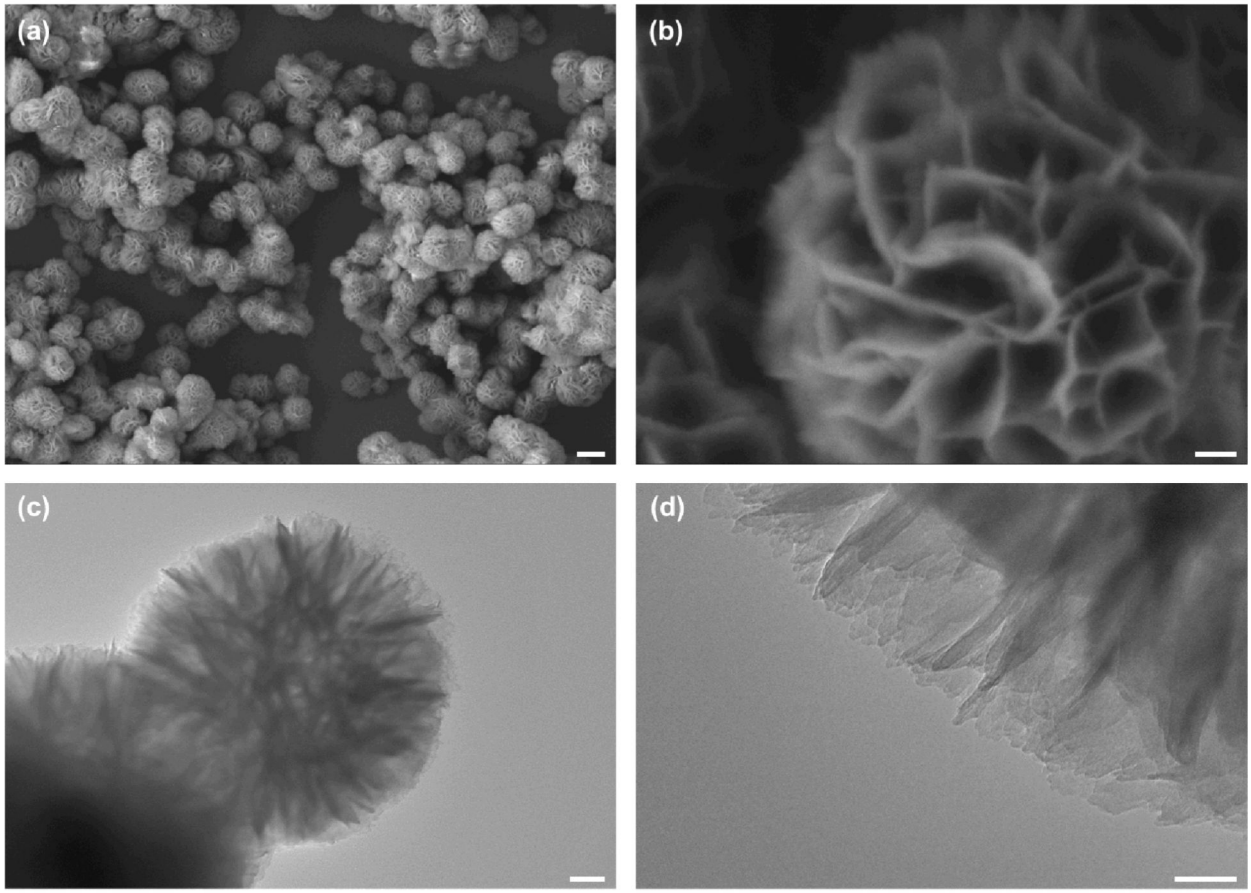

Figure 1.

Electron micrographs of MS-2 particles. (a) Low magnification SEM image of MS-2 (scale bar = 1 μm). (b) MS-2 particle viewed at higher magnification by SEM (scale bar = 100 nm). (c) TEM image of an MS-2 particle (scale bar = 100 nm). (d) TEM image showing the edge of an MS-2 particle viewed at higher magnification (scale bar = 50 nm).

NIH-PA Author Manuscript

NIH-PA Author Manuscript

NIH-PA Author Manuscript

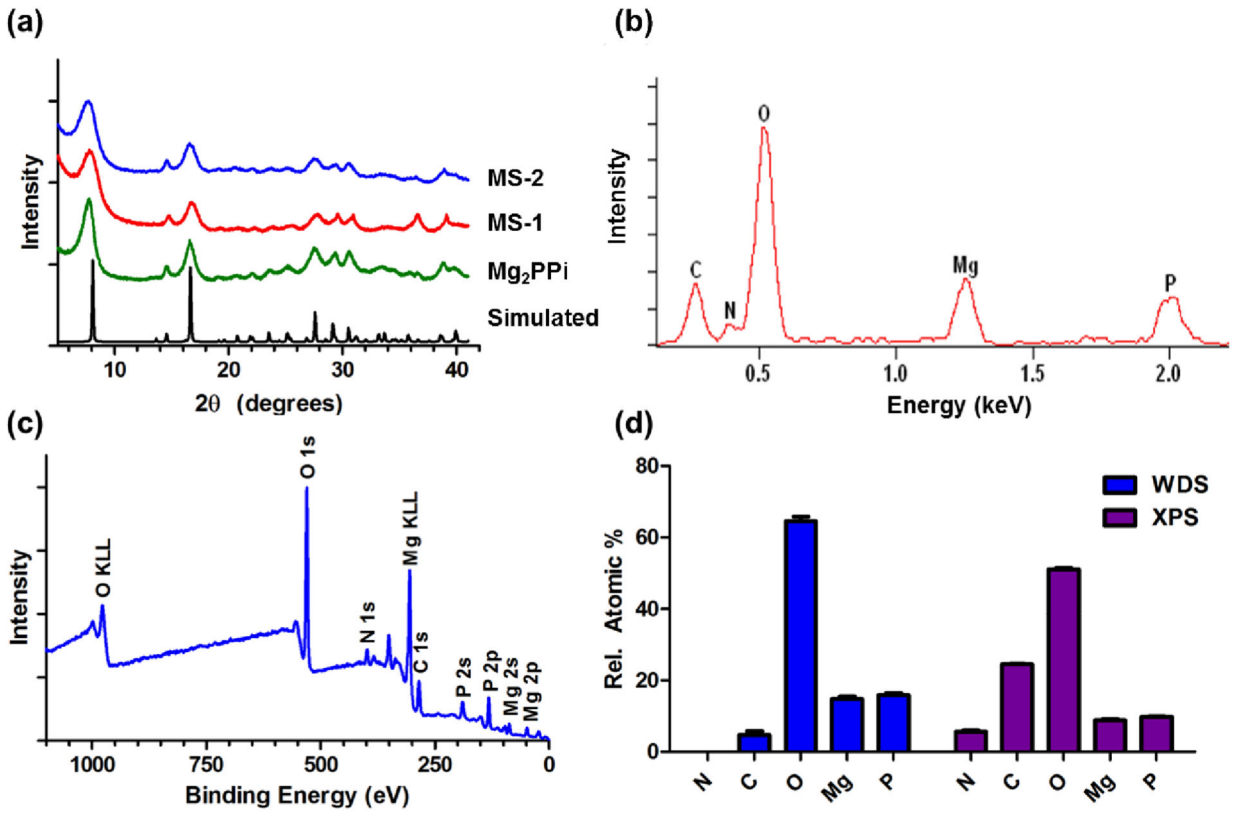

Figure 2.

X-ray diffraction and spectroscopic characterization of microsponge particles. (a) PXRD patterns for MS-2 (blue curve), MS-1 (red curve), magnesium pyrophosphate synthesized without RNA (green curve), and a simulated diffraction pattern for $Mg_2P_2O_7$•$3.5H_2O$ (black curve). (b) EDS spectrum obtained from point analysis of MS-2 microsponge particles. (c) XPS spectrum of an MS-2 sample. (d) Comparison of quantification results obtained for MS-2 usingWDS and XPS. Error bars represent mean ± SEM.

NIH-PA Author Manuscript
NIH-PA Author Manuscript
NIH-PA Author Manuscript

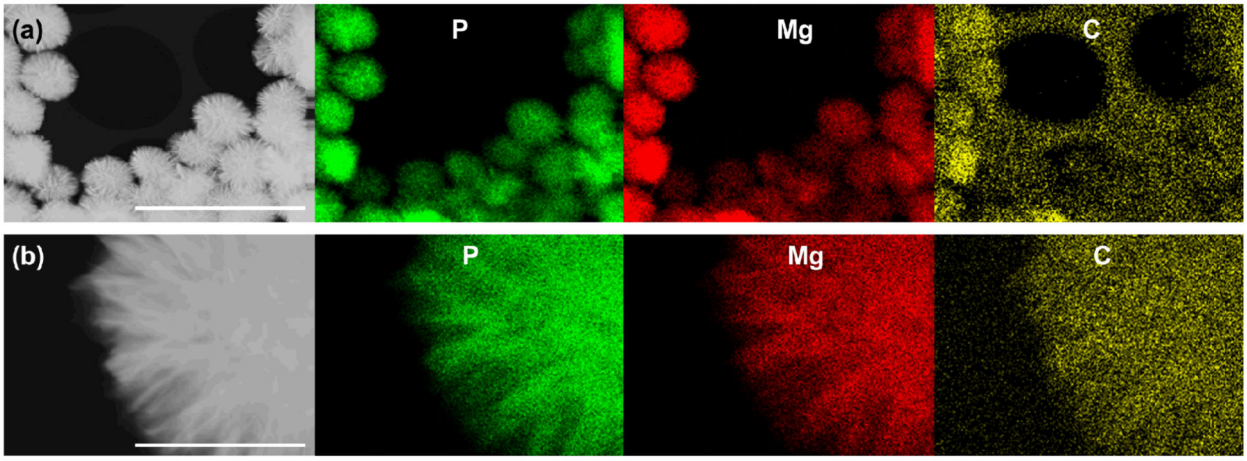

Figure 3.
STEM-based EDS mapping of MS-2 particles. (a) STEM image and EDS maps for MS-2 particles taken at low magnification (scale bar = 4 μm). (b) STEM image and EDS maps for an MS-2 particle at high magnification (scale bar = 600 nm).

NIH-PA Author Manuscript
NIH-PA Author Manuscript
NIH-PA Author Manuscript

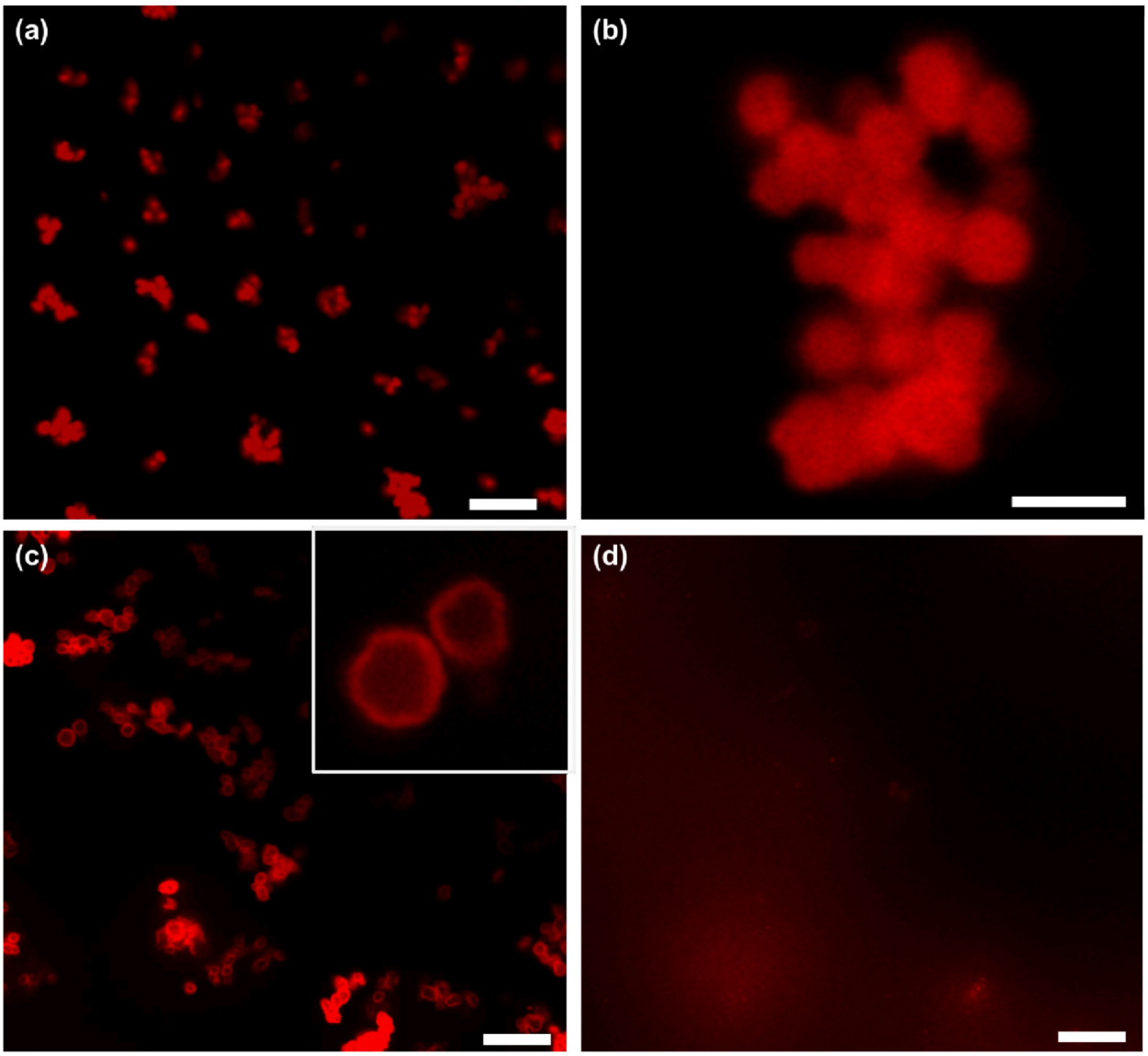

Figure 4.

Confocal fluorescence microscopy of microsponge particles synthesized in the presence of Cy5-labelled UTP. (a) Low magnification image of MS-2 particles (scale bar = 10 μm). (b) MS-2 particles viewed at higher magnification (scale bar = 3 μm). (c) MS-2 particles viewed 5 s after the addition of 5 mM EDTA (scale bar = 10 μm). Inset shows capsule structures after digital magnification. (d) Shows the same field of view as in (c), but 10 s after the addition of EDTA (scale bar = 10 μm).

NIH-PA Author Manuscript

NIH-PA Author Manuscript

NIH-PA Author Manuscript

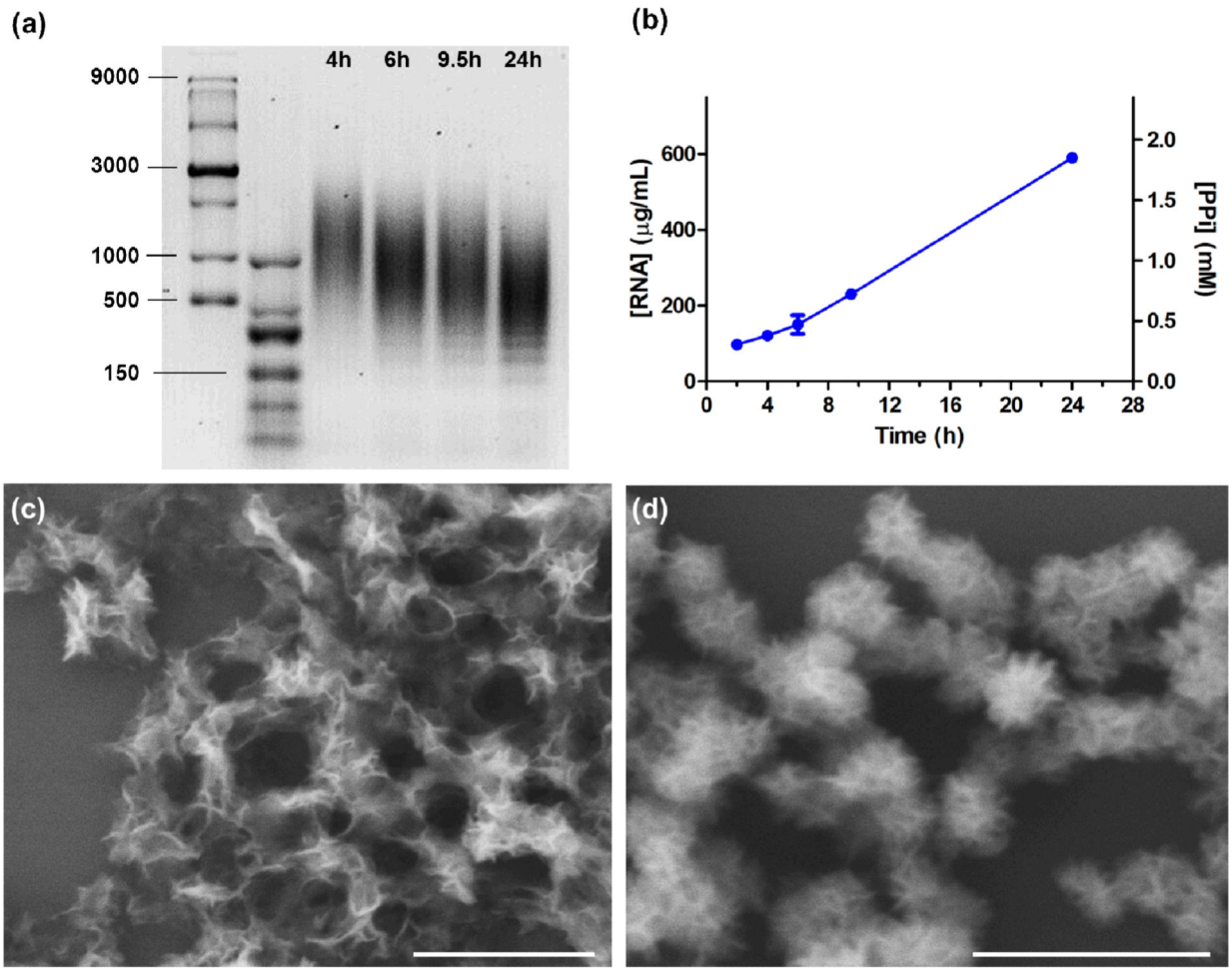

Figure 5.

Characterization of RCT reaction products from DNA-T2 at different time points. (a) Gel electrophoresis (1.5% agarose) of EDTA-treated particles isolated from an RCT reaction at different time points. (b) Quantification of RNA (ribogreen assay) produced from RCT reaction at different time points. PPi concentration (right y-axis) was calculated based on the measured RNA concentration. Error bars represent mean ± SEM (n = 3). (c) SEM image of the solid isolated from an RCT reaction after 4 h. (d) SEM image of solid isolated from an RCT reaction after 6 h. Scale bars are all equal to 1 μm.

NIH-PA Author Manuscript
NIH-PA Author Manuscript
NIH-PA Author Manuscript

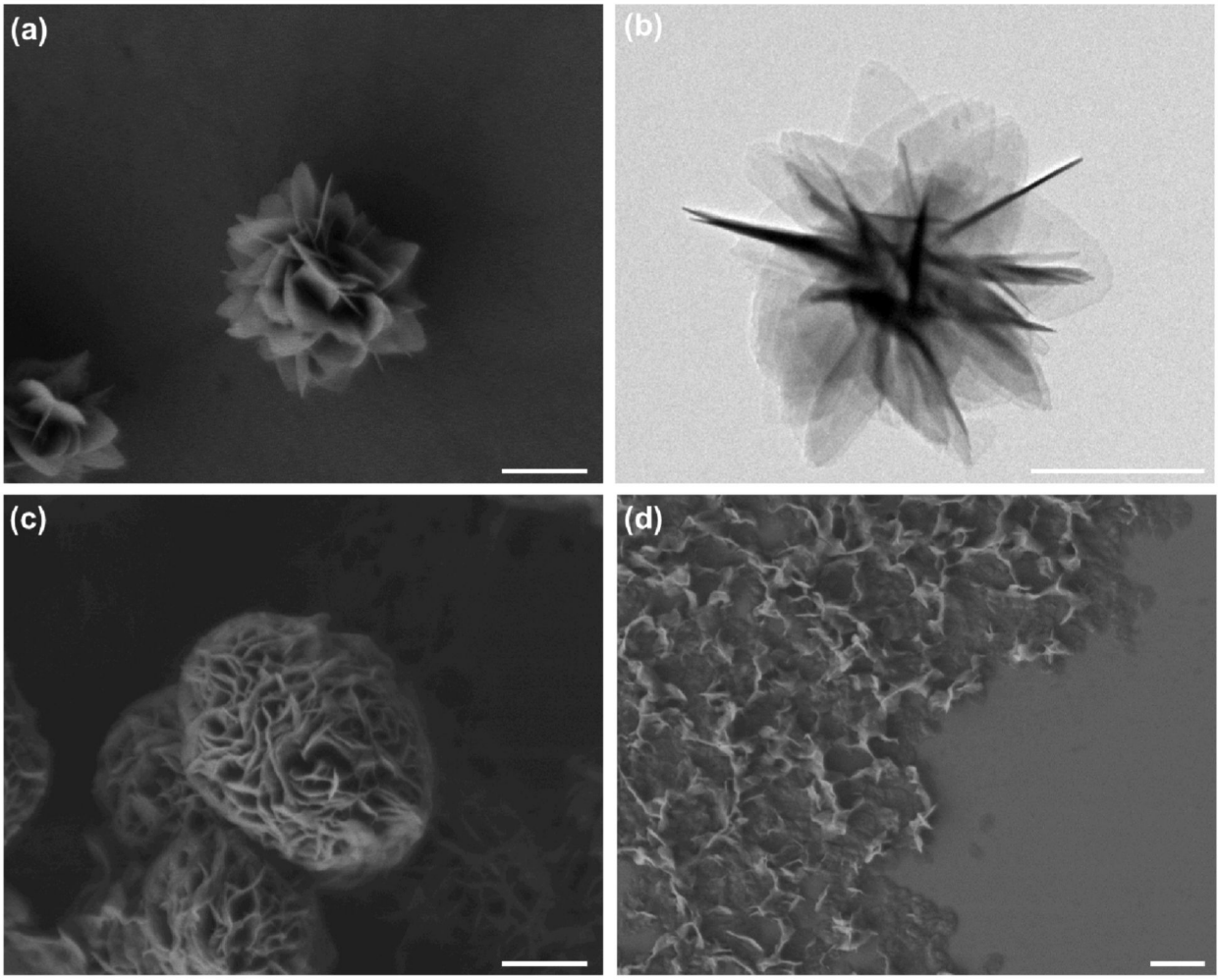

Figure 6.

Electron micrographs of magnesium pyrophosphate control samples formed with and without RNA. (a-b) SEM and TEM images of spherulitic Mg_2PPi-0.5 particles. (c-d) SEM images of an Mg_2PPi-0.5+RNA sample. All scale bars are equal to 1 μm.

NIH-PA Author Manuscript

NIH-PA Author Manuscript

NIH-PA Author Manuscript

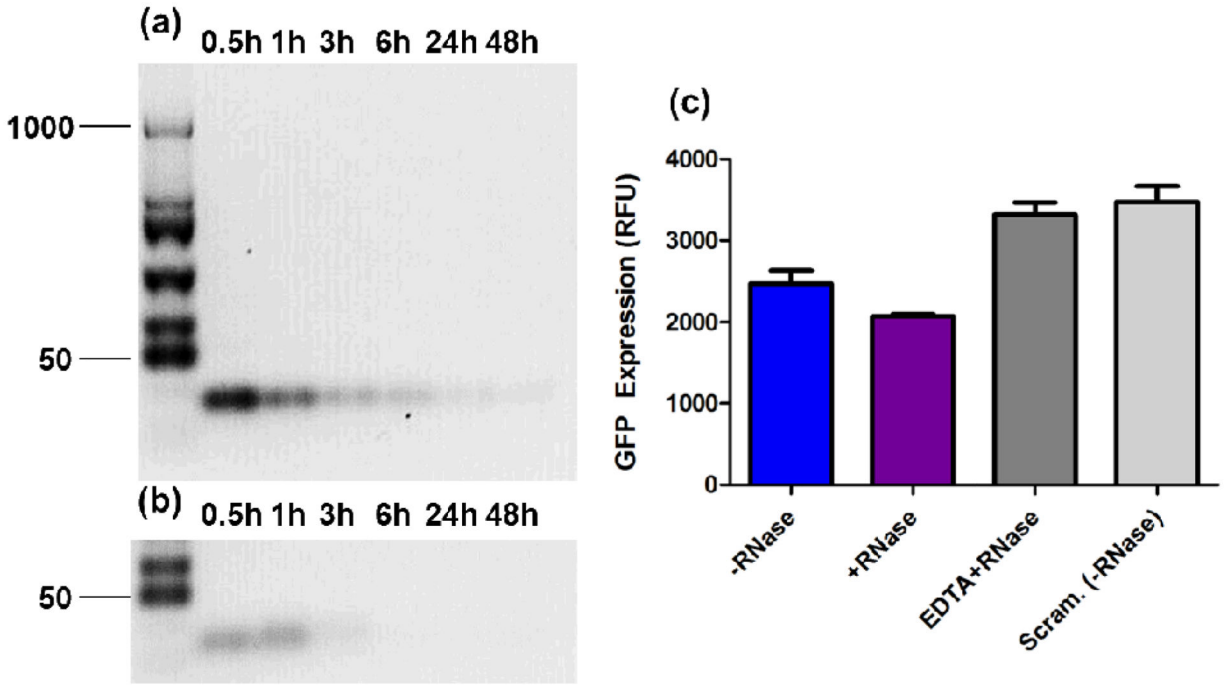

Figure 7.

Gel electrophoresis and transfection of MS-2 treated with RNase I_f. (a) Agarose gel electrophoresis of MS-2 sample treated with RNase I_f for different durations followed by treatment with EDTA. (b) Agarose gel electrophoresis of MS-2 sample dissolved with EDTA prior to being treated with RNase I_f for different durations. (c) Lipofectamine transfection of GFP-expressing SKOV3 cells using RNA released from GFP-targeted MS-2 particles (or a scrambled control), either before or after treatment with RNase I_f for 1 h. Error bars represent mean ± SEM (n = 3).

NIH-PA Author Manuscript

NIH-PA Author Manuscript

NIH-PA Author Manuscript

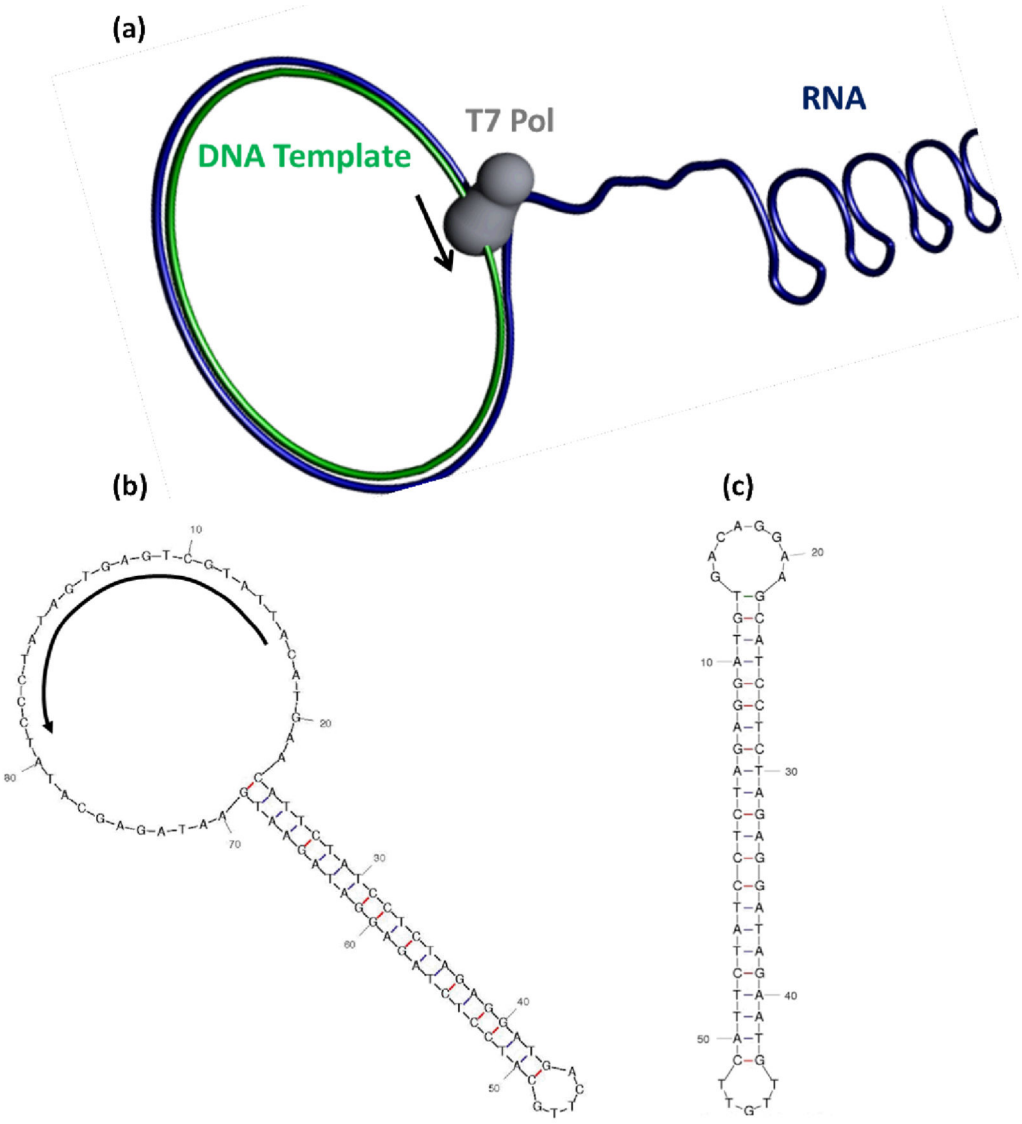

Scheme 1.

Components of the RCT reactions. (a) Cartoon illustrating RCT from a circular DNA template. (b) Sequence and secondary structure of DNA-T1 with the T7 promoter region highlighted by the curved arrow. (c) Sequence and secondary structure of DNA-T2.